Science Advances

AAAS

advances.sciencemag.org/cgi/content/full/4/2/eaao5508/DC1

Supplementary Materials for

Mapping a functional cancer genome atlas of tumor suppressors in mouse liver using AAV-CRISPR–mediated direct in vivo screening

Guangchuan Wang, Ryan D. Chow, Lupeng Ye, Christopher D. Guzman, Xiaoyun Dai, Matthew B. Dong, Feng Zhang, Phillip A. Sharp, Randall J. Platt, Sidi Chen

Published 28 February 2018, *Sci. Adv.* **4**, eaao5508 (2018)
DOI: 10.1126/sciadv.aao5508

The PDF file includes:

Other Supplementary Material for this manuscript includes the following:
(available at advances.sciencemag.org/cgi/content/full/4/2/eaao5508/DC1)

- table S1 (Microsoft Excel format). DNA sequences of sgRNA spacers in mTSG library.
- table S2 (Microsoft Excel format). Raw read counts of mTSG plasmid library.
- table S3 (Microsoft Excel format). Tumor volume data as measured by MRI.
- table S4 (Microsoft Excel format). Survival data for PBS-, vector-, or mTSG-treated animals.
- table S5 (Microsoft Excel format). Tumor area data as measured by tissue histology.
- table S6 (Microsoft Excel format). Sequence information and annotation for all MIPs used in the study.
- table S7 (Microsoft Excel format). Metadata for all of the 133 sequenced samples.
- table S8 (Microsoft Excel format). MIP capture sequencing coverage statistics across all predicted cutting sites of sgRNAs in AAV-mTSG library.
- table S9 (Microsoft Excel format). Raw indel variant calls of all samples with targeted capture sequencing before filtering.
- table S10 (Microsoft Excel format). sgRNA-level sum indel frequency table for all samples with targeted capture sequencing.
- table S11 (Microsoft Excel format). sgRNA-level binary MS calls in livers from mice treated with AAV-mTSG library.
- table S12 (Microsoft Excel format). Gene-level binary MG calls in livers from mice treated with AAV-mTSG library.
- table S13 (Microsoft Excel format). Co-occurrence analysis of MG pairs in livers from mice treated with AAV-mTSG library.
- table S14 (Microsoft Excel format). Correlation analysis of gene-level sum indel frequency in livers from mice treated with AAV-mTSG library.
- table S15 (Microsoft Excel format). Mutant frequencies for all unique variants present across all mTSG liver samples.
- table S16 (Microsoft Excel format). Spearman rank correlation matrix for five individual liver lobes within a single mouse.
- table S17 (Microsoft Excel format). Mutant frequencies for all unique variants present in five individual liver lobes from a single mouse.

Figure S1

A

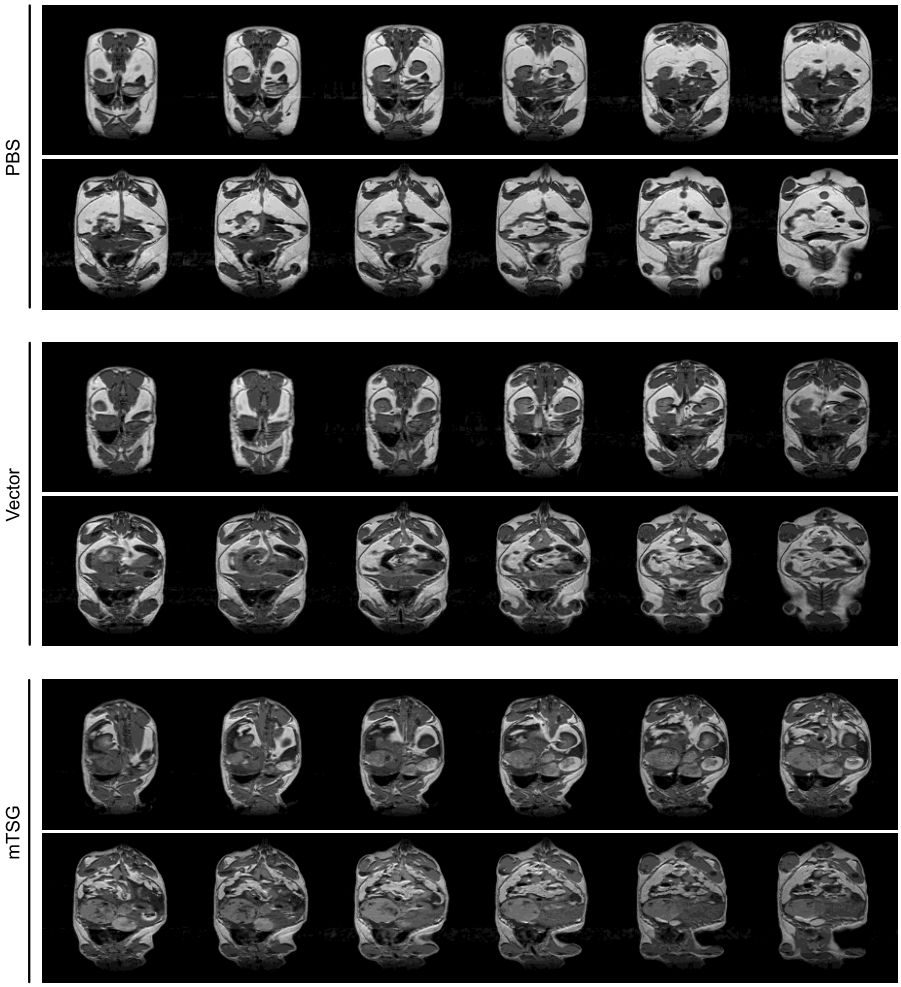
PBS
Vector
mTSG

B

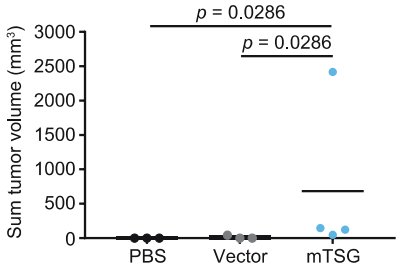
p = 0.0286
p = 0.0286
Sum tumor volume (mm³)
3000
2500
2000
1500
1000
500
0
PBS
Vector
mTSG

fig. S1. Representative full-spectrum MRI series of livers from PBS, vector and mTSG-treated mice. (**A**) Full-spectrum MRI slices from representative PBS, vector, and mTSG-treated mice. (**B**) Dot plot of the sum tumor volume per mouse (in mm^3) in mice treated with PBS (black, n = 3), vector (gray, n = 3), or mTSG library (blue, n = 4). mTSG-treated mice had significantly higher tumor burdens than PBS (one-sided Mann-Whitney test, $p = 0.0286$) or vector-treated animals ($p = 0.0286$).

Figure S2

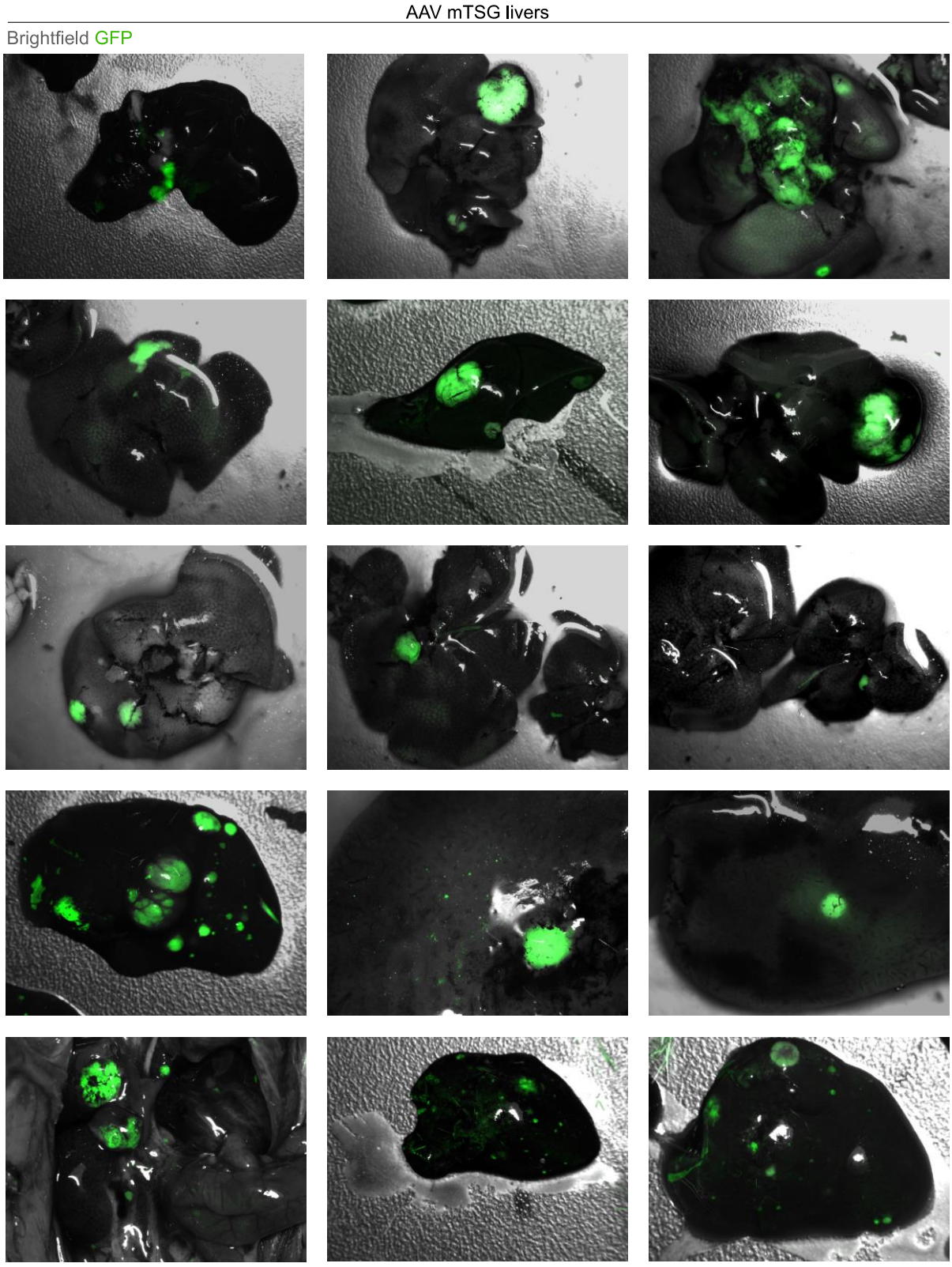

fig. S2. Additional brightfield images of mTSG-treated livers with GFP overlay. Additional brightfield images with GFP fluorescence overlay (green) of livers from 15 mTSG-treated mice at the time of sacrifice.

Figure S3

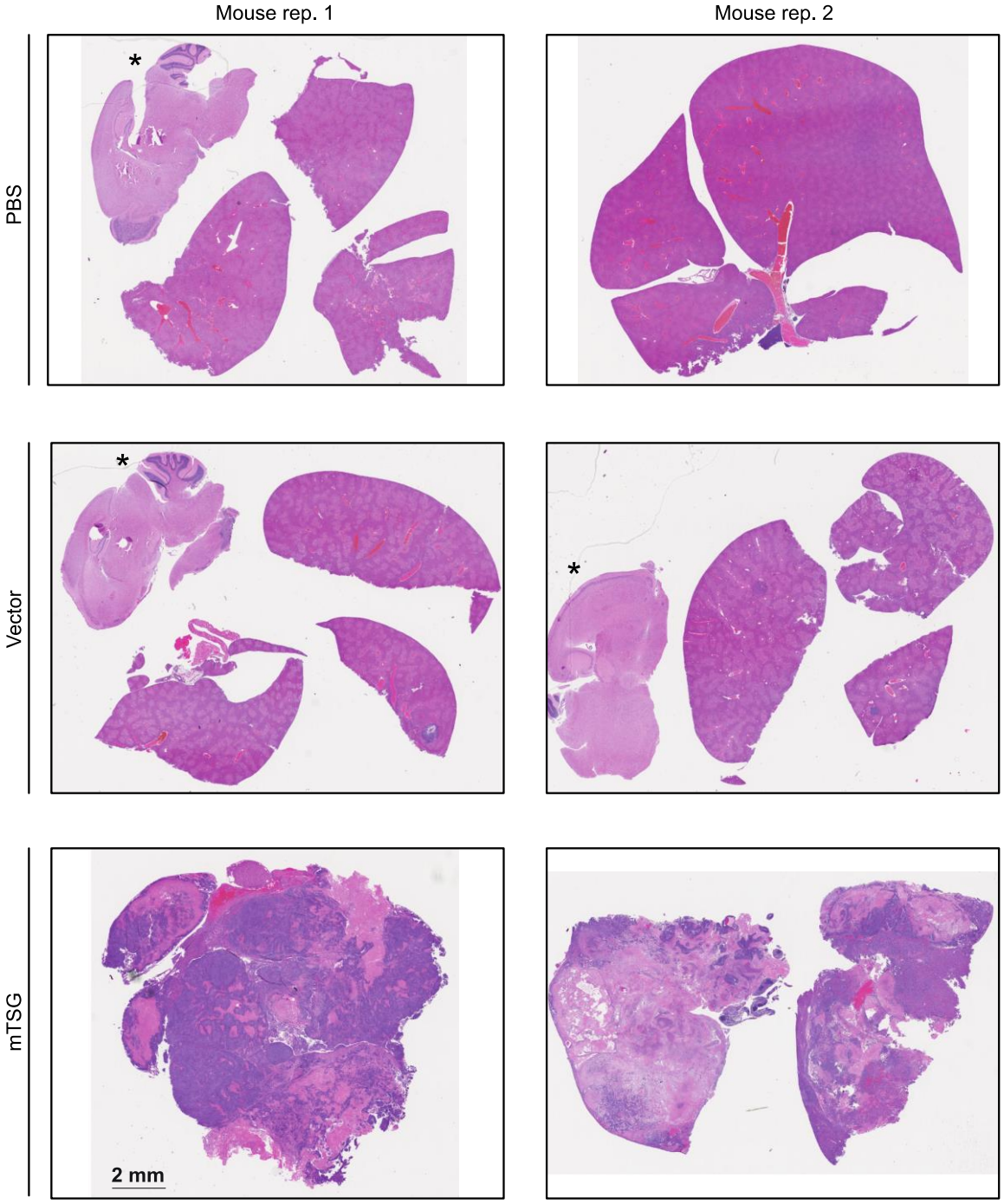

fig. S3. Representative full-slide scanning images of mouse liver sections in PBS, vector, and mTSG treatment groups. Full slide scans of liver sections from PBS, vector and mTSG-treated mice. Two representative mice from each group are shown. Some brain sections are also present in the same scanned field, noted with asterisks. PBS samples did not have any detectable nodules, while vector-treated samples occasionally had developed small nodules. In contrast, mTSG-treated samples were replete with tumors. Scale bar is 2 mm.

Figure S4

A

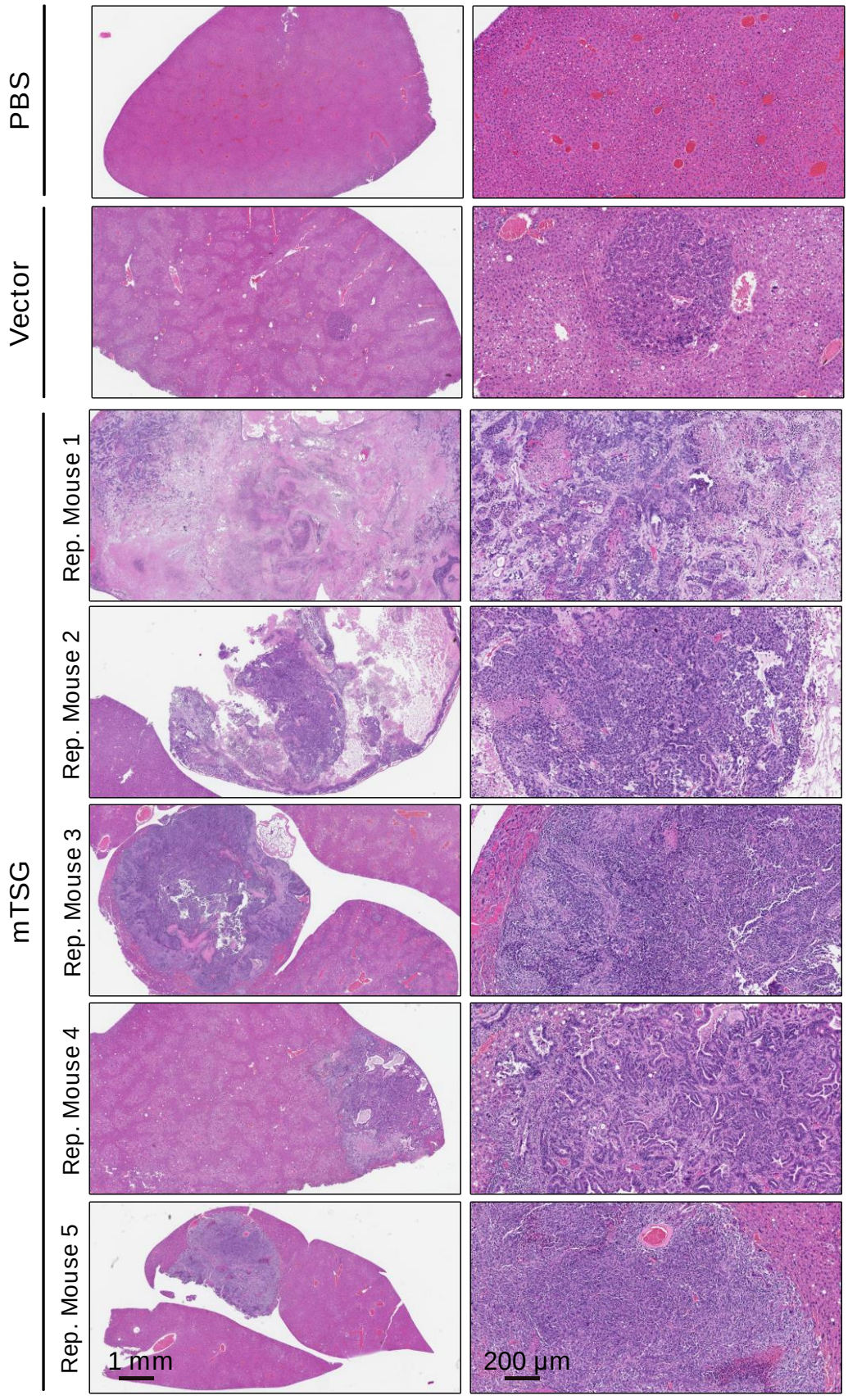
PBS
Vector
mTSG
Rep. Mouse 1
Rep. Mouse 2
Rep. Mouse 3
Rep. Mouse 4
Rep. Mouse 5
1 mm
200 µm

Figure S4 continued

B

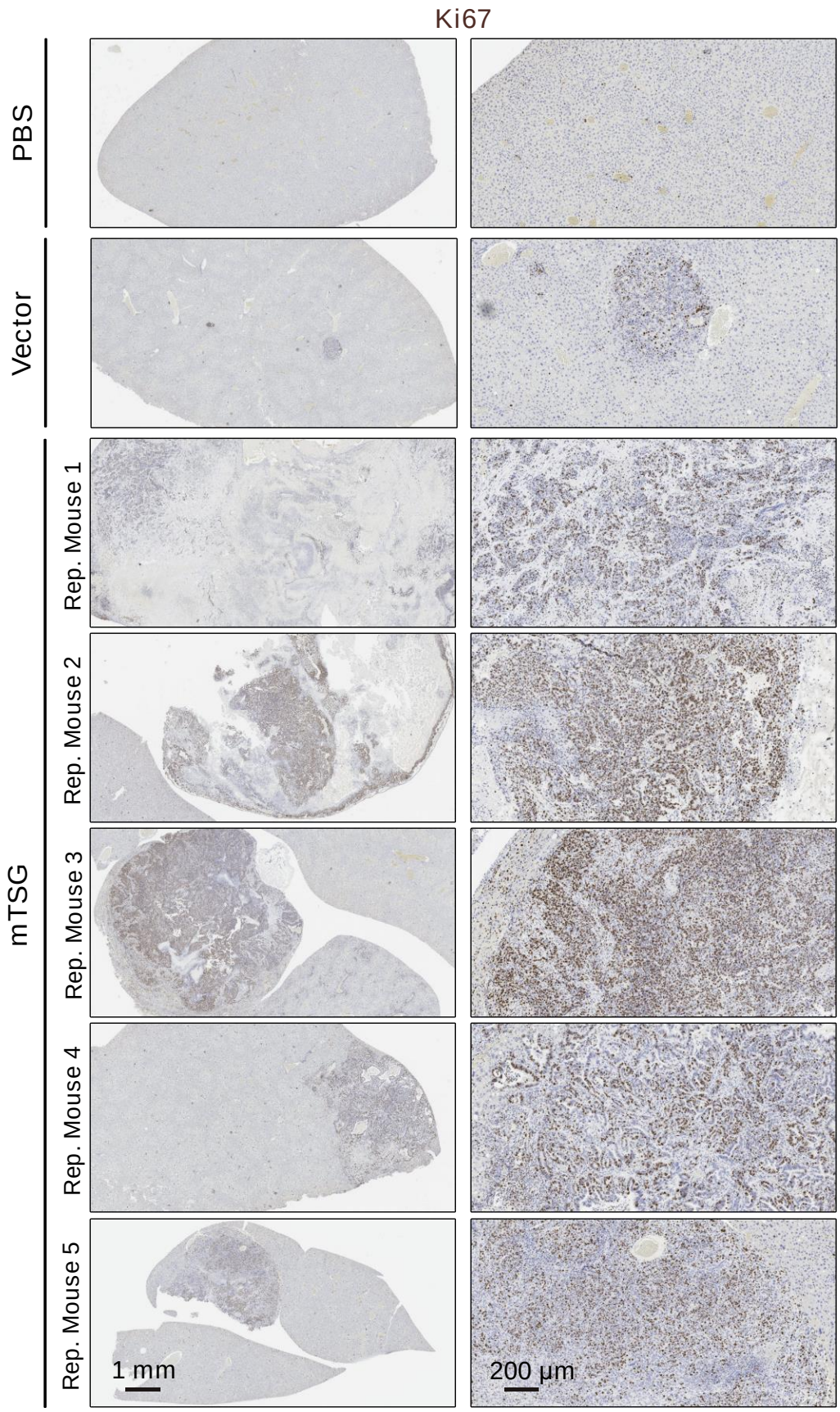

Figure S4 continued

C

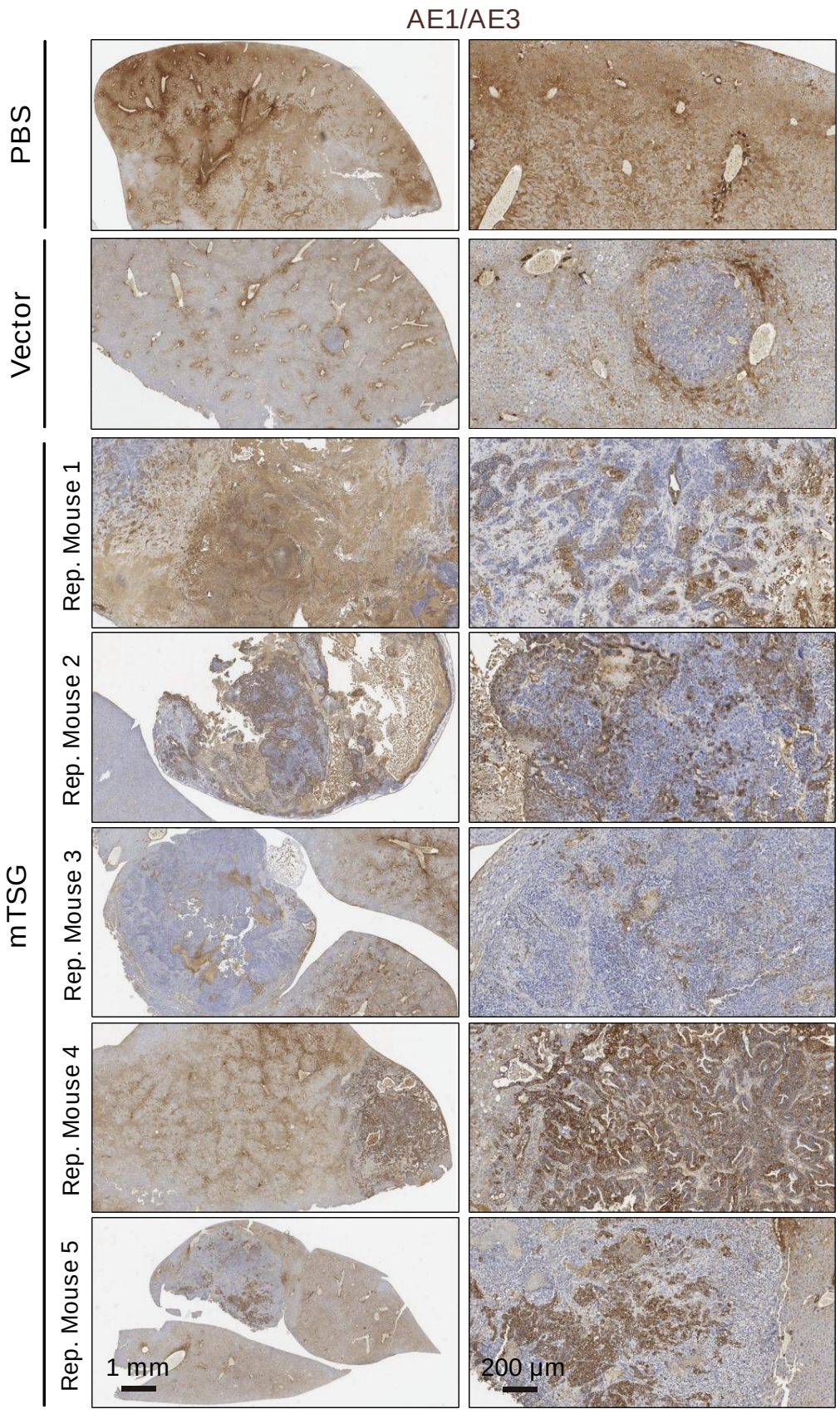

fig. S4. Representative histology and immunohistochemistry images of mouse liver sections in PBS, vector, and mTSG groups. (**A**) Representative liver sections from PBS, vector, and mTSG-treated mice with hematoxylin and eosin staining. The vector sample and mTSG replicate 4 pictured here are from the same mice shown in Figure 2D. Scale bar is 1 mm for low magnification images, 200 μm for high magnification images. (**B**) Representative liver sections from PBS, vector, and mTSG-treated mice with Ki67 staining. Sections correspond to the same mice shown in Fig. S4A. Scale bar is 1 mm for low magnification images, 200 μm for high magnification images. (**C**) Representative liver sections from PBS, vector, and mTSG-treated mice with pan-cytokeratin AE1/AE3 staining. Sections correspond to the same mice shown in fig. S4A. Scale bar is 1 mm for low magnification images, 200 μm for high magnification images.

Figure S5

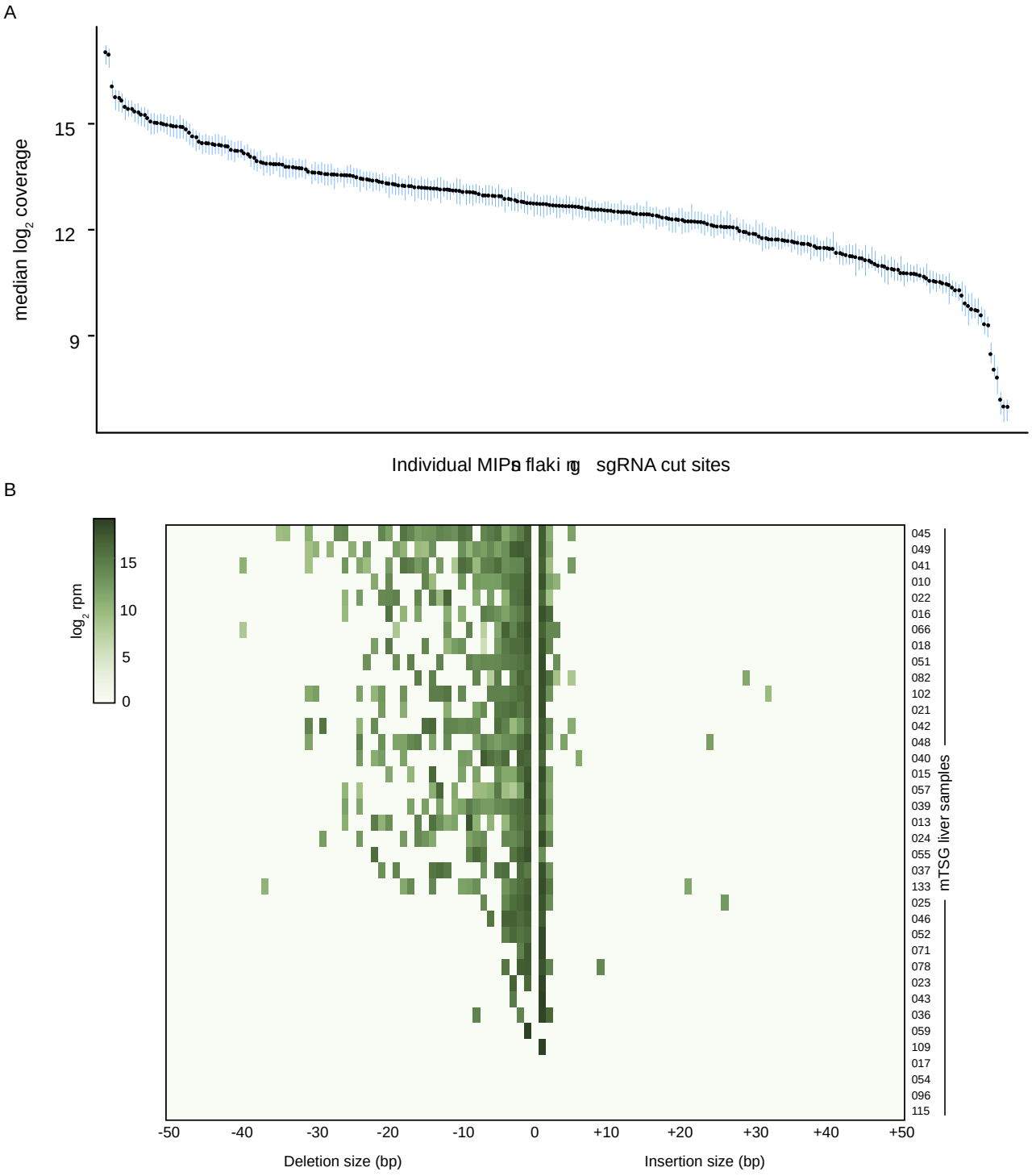
A
median log2 coverage
15
12
9
Individual MIPs flanking sgRNA cut sites
B
log2 rpm
15
10
5
0
mTSG liver samples
045
049
041
010
022
016
066
018
051
082
102
021
042
048
040
015
057
039
013
024
055
037
133
025
046
052
071
078
023
043
036
059
109
017
054
096
115
-50
-40
-30
-20
-10
0
+10
+20
+30
+40
+50
Deletion size (bp)
Insertion size (bp)

fig. S5. MIP capture sequencing statistics and indel size distribution of mTSG livers. (**A**) Plot of median $\log_2$ sequencing coverage across all sequenced samples in amplicons targeted by the 266 MIPs (black dots). MIPs were designed to amplify the genomic regions flanking the predicted cut sites of each sgRNA. 95% confidence intervals for the median are depicted with blue lines. Median read depth across all MIPs approximated a lognormal distribution, indicating relatively even capture of the target loci. (**B**) Heat map detailing indel size distribution and abundance across all mutated sgRNA sites from mTSG-treated liver samples. Positive indel sizes denote insertions, while negative indel sizes indicate deletions. Depicted values are in terms of total log2 normalized reads per million (rpm) for each sample. Most variant reads are deletions (80.8%) compared to insertions (19.2%).

Figure S6

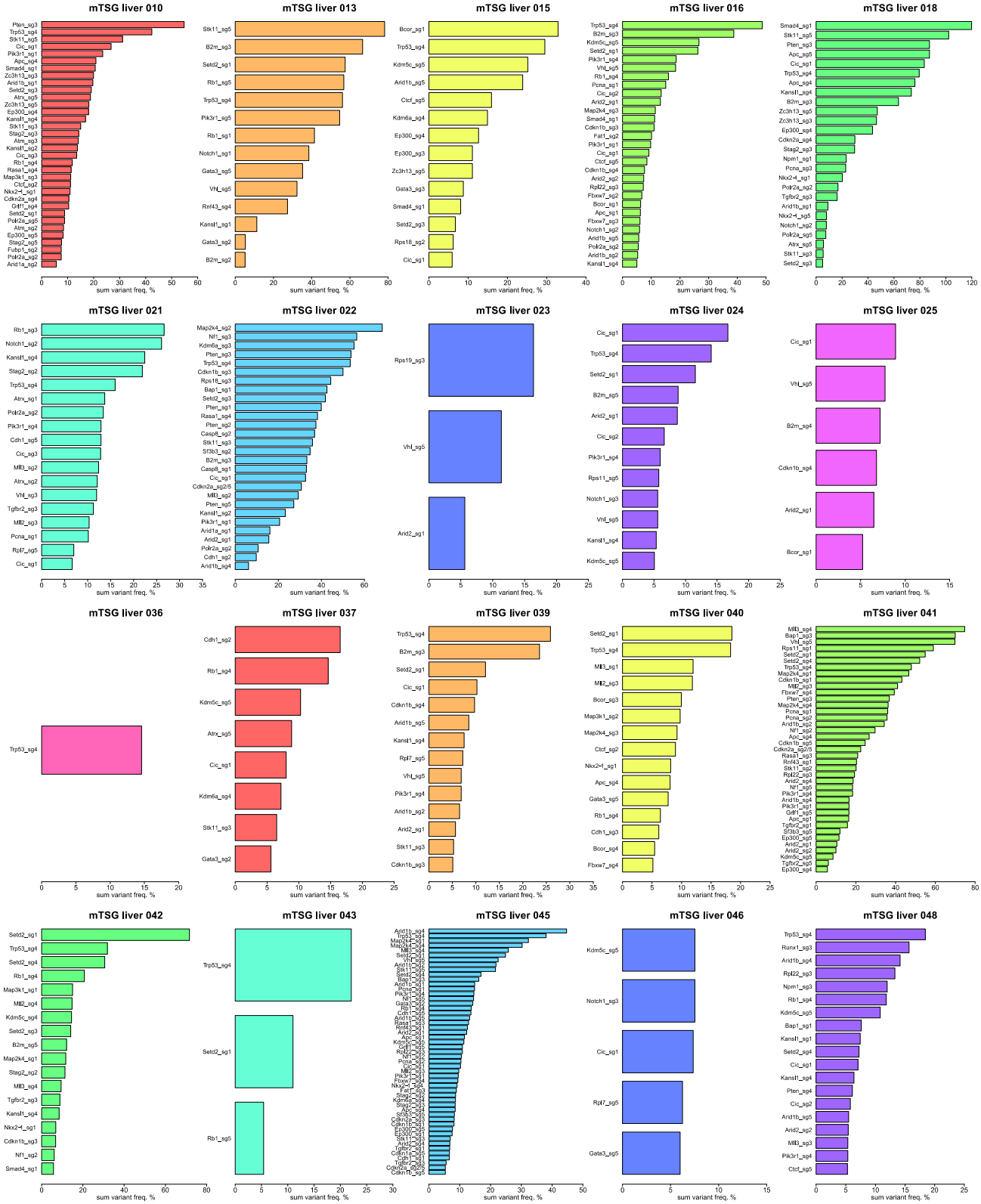
mTSG liver 010
Pten_sg3
Trp53_sg4
Stk11_sg5
Cic_sg1
Pik3r1_sg1
Apc_sg4
Smad4_sg1
Zc3h13_sg3
Arid1b_sg1
Setd2_sg3
Atrx_sg5
Zc3h13_sg5
Ep300_sg4
Kansl1_sg4
Stk11_sg3
Stag2_sg3
Atm_sg3
Kansl1_sg2
Cic_sg3
Rb1_sg4
Rasa1_sg4
Map3k1_sg3
Ctcf_sg2
Nkx2-4_sg1
Cdkn2a_sg4
Gtf1_sg4
Setd2_sg1
Polr2a_sg5
Atm_sg2
Ep300_sg5
Stag2_sg5
Fubp1_sg2
Polr2a_sg2
Arid1a_sg2
sum variant freq. %
mTSG liver 013
Stk11_sg5
B2m_sg3
Setd2_sg1
Rb1_sg5
Trp53_sg4
Pik3r1_sg5
Rb1_sg1
Notch1_sg1
Gata3_sg5
Vhl_sg5
Rnf43_sg4
Kansl1_sg1
Gata3_sg2
B2m_sg2
sum variant freq. %
mTSG liver 015
Bcor_sg1
Trp53_sg4
Kdm5c_sg5
Arid1b_sg5
Ctcf_sg5
Kdm6a_sg4
Ep300_sg4
Ep300_sg3
Zc3h13_sg5
Gata3_sg3
Smad4_sg1
Setd2_sg3
Rps18_sg2
Cic_sg1
sum variant freq. %
mTSG liver 016
Trp53_sg4
B2m_sg3
Kdm5c_sg5
Setd2_sg1
Pik3r1_sg4
Vhl_sg5
Rb1_sg4
Pcna_sg1
Cic_sg2
Arid2_sg1
Map2k4_sg3
Smad4_sg1
Cdkn1b_sg3
Fat1_sg2
Pik3r1_sg1
Cic_sg1
Ctcf_sg5
Cdkn1b_sg4
Arid2_sg2
Rpl22_sg3
Fbxw7_sg2
Bcor_sg1
Apc_sg1
Fbxw7_sg3
Notch1_sg2
Arid1b_sg3
Polr2a_sg2
Arid1b_sg2
Kansl1_sg4
sum variant freq. %
mTSG liver 018
Smad4_sg1
Stk11_sg5
Pten_sg3
Apc_sg5
Cic_sg1
Trp53_sg4
Apc_sg4
Kansl1_sg4
B2m_sg3
Zc3h13_sg5
Zc3h13_sg3
Ep300_sg4
Cdkn2a_sg4
Stag2_sg3
Npm1_sg1
Pcna_sg3
Nkx2-4_sg1
Polr2a_sg2
Tgfbr2_sg3
Arid1b_sg1
Nkx2-4_sg5
Notch1_sg2
Polr2a_sg5
Atrx_sg5
Stk11_sg3
Setd2_sg3
sum variant freq. %
mTSG liver 021
Rb1_sg3
Notch1_sg2
Kansl1_sg4
Stag2_sg2
Trp53_sg4
Atrx_sg1
Polr2a_sg2
Pik3r1_sg4
Cdh1_sg5
Cic_sg3
Mll3_sg2
Atrx_sg2
Vhl_sg3
Tgfbr2_sg3
Mll2_sg3
Pcna_sg1
Rpl7_sg5
Cic_sg1
sum variant freq. %
mTSG liver 022
Map2k4_sg2
Nf1_sg3
Kdm6a_sg3
Pten_sg3
Trp53_sg4
Cdkn1b_sg3
Rps18_sg3
Bap1_sg1
Setd2_sg3
Pten_sg1
Rasa1_sg4
Pten_sg2
Casp8_sg2
Stk11_sg3
Sf3b3_sg2
B2m_sg3
Casp8_sg1
Cic_sg1
Cdkn2a_sg2/5
Mll3_sg2
Pten_sg5
Kansl1_sg2
Pik3r1_sg1
Arid1a_sg1
Arid2_sg1
Polr2a_sg2
Cdh1_sg2
Arid1b_sg4
sum variant freq. %
mTSG liver 023
Rps19_sg3
Vhl_sg5
Arid2_sg1
sum variant freq. %
mTSG liver 024
Cic_sg1
Trp53_sg4
Setd2_sg1
B2m_sg5
Arid2_sg1
Cic_sg2
Pik3r1_sg4
Rps11_sg5
Notch1_sg3
Vhl_sg5
Kansl1_sg4
Kdm5c_sg5
sum variant freq. %
mTSG liver 025
Cic_sg1
Vhl_sg5
B2m_sg4
Cdkn1b_sg4
Arid2_sg1
Bcor_sg1
sum variant freq. %
mTSG liver 036
Trp53_sg4
sum variant freq. %
mTSG liver 037
Cdh1_sg2
Rb1_sg4
Kdm5c_sg5
Atrx_sg5
Cic_sg1
Kdm6a_sg4
Stk11_sg3
Gata3_sg2
sum variant freq. %
mTSG liver 039
Trp53_sg4
B2m_sg3
Setd2_sg1
Cic_sg1
Cdkn1b_sg4
Arid1b_sg5
Kansl1_sg4
Rpl7_sg5
Vhl_sg5
Pik3r1_sg4
Arid1b_sg2
Arid2_sg1
Stk11_sg3
Cdkn1b_sg3
sum variant freq. %
mTSG liver 040
Setd2_sg1
Trp53_sg4
Mll3_sg1
Mll2_sg3
Bcor_sg3
Map3k1_sg2
Map2k4_sg3
Ctcf_sg2
Nkx2-4_sg1
Apc_sg4
Gata3_sg5
Rb1_sg4
Cdh1_sg3
Bcor_sg4
Fbxw7_sg4
sum variant freq. %
mTSG liver 041
Mll3_sg4
Bap1_sg3
Vhl_sg5
Rps11_sg1
Setd2_sg1
Setd2_sg4
Trp53_sg4
Map2k4_sg1
Cdkn1b_sg1
Mll2_sg3
Fbxw7_sg4
Pten_sg3
Map2k4_sg4
Pcna_sg1
Pcna_sg2
Arid1b_sg2
Nf1_sg2
Apc_sg4
Cdkn1b_sg5
Cdkn2a_sg2/5
Rasa1_sg3
Rnf43_sg1
Stk11_sg2
Rpl22_sg3
Arid2_sg4
Nf1_sg5
Pik3r1_sg4
Arid1b_sg4
Pik3r1_sg1
Gtf1_sg5
Apc_sg1
Tgfbr2_sg1
Sf3b3_sg5
Ep300_sg5
Arid2_sg3
Arid2_sg2
Kdm5c_sg5
Tgfbr2_sg5
Ep300_sg4
sum variant freq. %
mTSG liver 042
Setd2_sg1
Trp53_sg4
Setd2_sg4
Rb1_sg4
Map3k1_sg1
Mll2_sg4
Kdm5c_sg4
Setd2_sg3
B2m_sg5
Map2k4_sg1
Stag2_sg2
Mll3_sg4
Tgfbr2_sg3
Kansl1_sg4
Nkx2-4_sg1
Cdkn1b_sg3
Nf1_sg2
Smad4_sg1
sum variant freq. %
mTSG liver 043
Trp53_sg4
Setd2_sg1
Rb1_sg5
sum variant freq. %
mTSG liver 045
Arid1b_sg4
Trp53_sg4
Map2k4_sg1
Map2k4_sg4
Mll3_sg4
Setd2_sg1
Arid1b_sg5
Stk11_sg5
Setd2_sg4
Bap1_sg3
Arid1b_sg1
Pcna_sg1
Pik3r1_sg4
Nf1_sg5
Gata3_sg2
Cic_sg4
Arid1b_sg3
Rasa1_sg3
Rnf43_sg1
Arid2_sg4
Apc_sg1
Kdm5c_sg2
Cdh1_sg5
Polr2a_sg3
Mll2_sg3
Pik3r1_sg1
Fbxw7_sg4
Nkx2-4_sg4
Fat1_sg3
Stag2_sg2
Kdm6a_sg4
Stag2_sg3
Apc_sg4
Sf3b3_sg3
Cdkn2a_sg3
Cdkn1b_sg2
Ep300_sg3
Ep300_sg2
Stk11_sg3
Arid2_sg3
Tgfbr2_sg1
Cdkn1a_sg5
Cdh1_sg1
Tgfbr2_sg2
Cdkn2a_sg5
Cdkn1b_sg5
sum variant freq. %
mTSG liver 046
Kdm5c_sg5
Notch1_sg3
Cic_sg1
Rpl7_sg5
Gata3_sg5
sum variant freq. %
mTSG liver 048
Trp53_sg4
Runx1_sg3
Arid1b_sg4
Rpl22_sg3
Npm1_sg3
Rb1_sg4
Kdm5c_sg5
Bap1_sg1
Kansl1_sg1
Setd2_sg4
Cic_sg1
Kansl1_sg4
Pten_sg4
Cic_sg2
Arid1b_sg5
Arid2_sg2
Mll3_sg3
Pik3r1_sg4
Ctcf_sg5
sum variant freq. %

Figure S6 continued

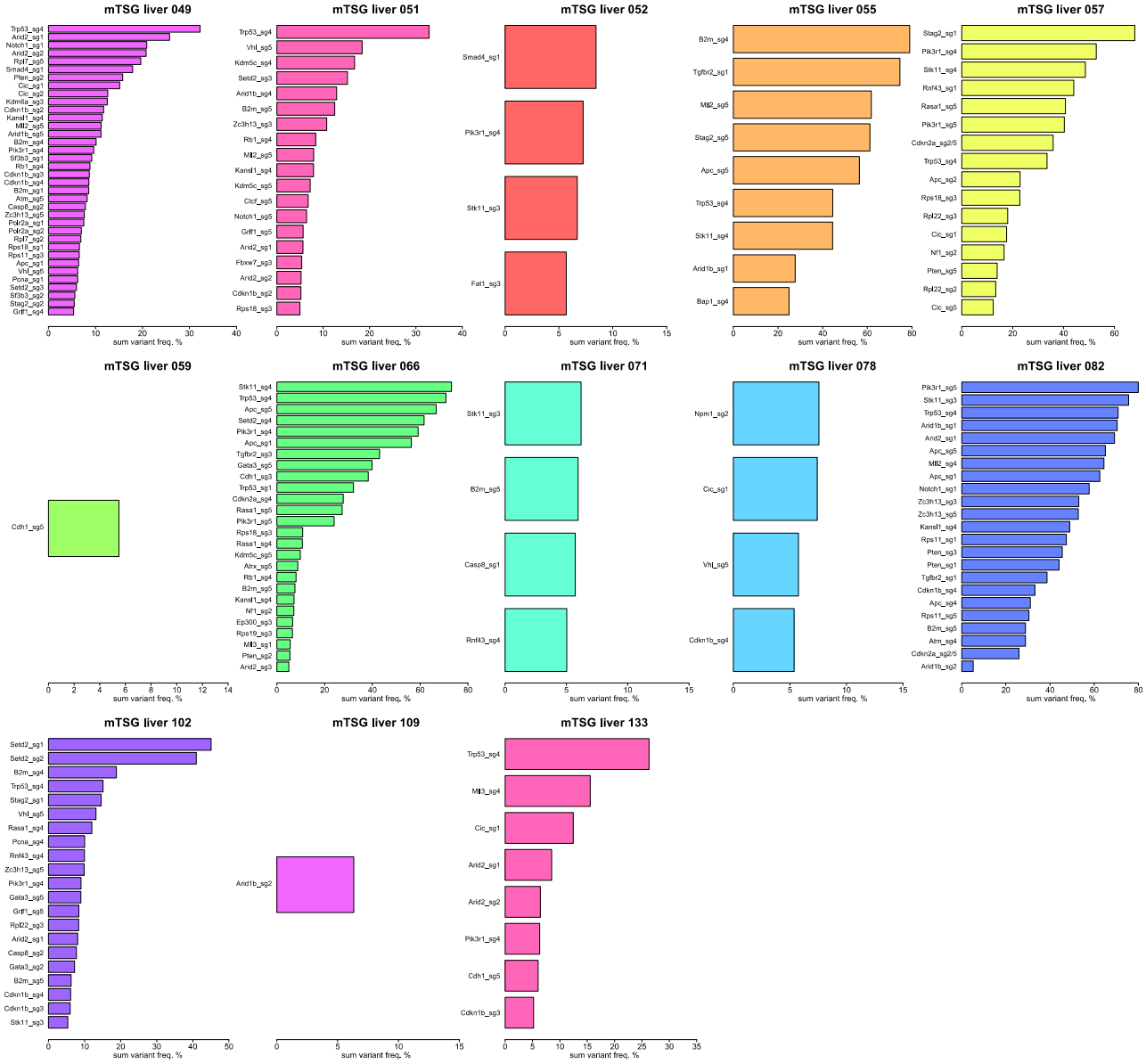

fig. S6. Mutated sgRNA sites across all liver samples from mice treated with AAV-mTSG library. Waterfall plots of mutated sgRNA sites across all 33 mTSG-treated liver samples, sorted by sum variant frequency. Four samples (mTSG liver 17, mTSG liver 54, mTSG liver 96 and mTSG liver 115) are not shown, as these samples were not found to have any mutated sgRNA sites per our stringent variant calling strategy. The extensive mutational heterogeneity amongst the liver samples is suggestive of strong positive selective forces acting on diverse loss-of-function mutations induced by the mTSG library.

Figure S7

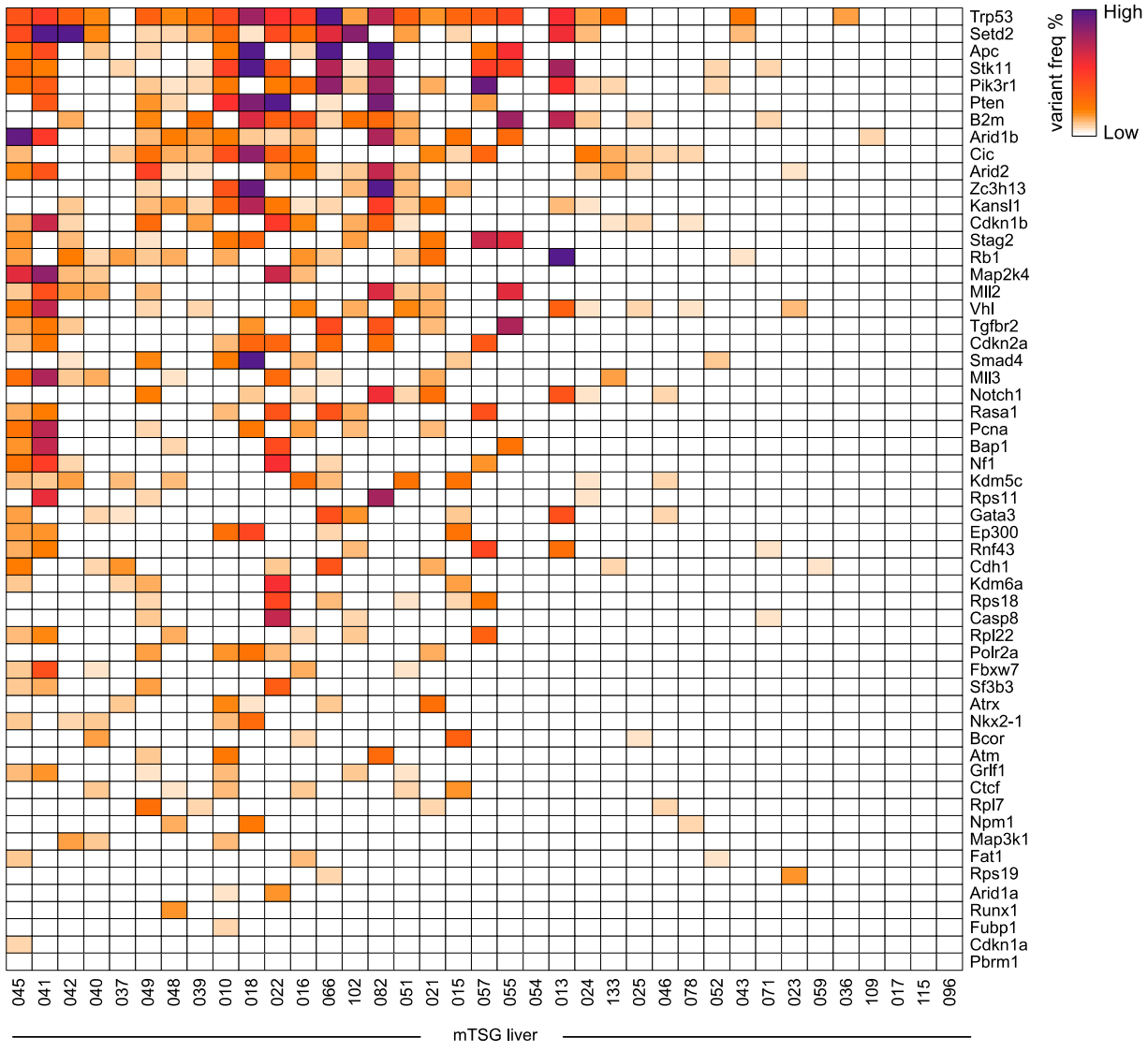
Trp53
Setd2
Apc
Stk11
Pik3r1
Pten
B2m
Arid1b
Cic
Arid2
Zc3h13
Kansl1
Cdkn1b
Stag2
Rb1
Map2k4
Mll2
Vhl
Tgfbr2
Cdkn2a
Smad4
Mll3
Notch1
Rasa1
Pcna
Bap1
Nf1
Kdm5c
Rps11
Gata3
Ep300
Rnf43
Cdh1
Kdm6a
Rps18
Casp8
Rpl22
Polr2a
Fbxw7
Sf3b3
Atrx
Nkx2-1
Bcor
Atm
Grlf1
Ctcf
Rpl7
Npm1
Map3k1
Fat1
Rps19
Arid1a
Runx1
Fubp1
Cdkn1a
Pbrm1
variant freq %
High
Low
045
041
042
040
037
049
048
039
010
018
022
016
066
102
082
051
021
015
057
055
054
013
024
133
025
046
078
052
043
071
023
059
036
109
017
115
096
mTSG liver

fig. S7. Heat map of gene-level sum variant frequency across all mTSG liver samples. Heat map depicting sum variant frequencies for the 56 genes represented in the library, across all mTSG liver samples. Genes are ordered according to average sum variant frequency (top to bottom row).

Figure S8

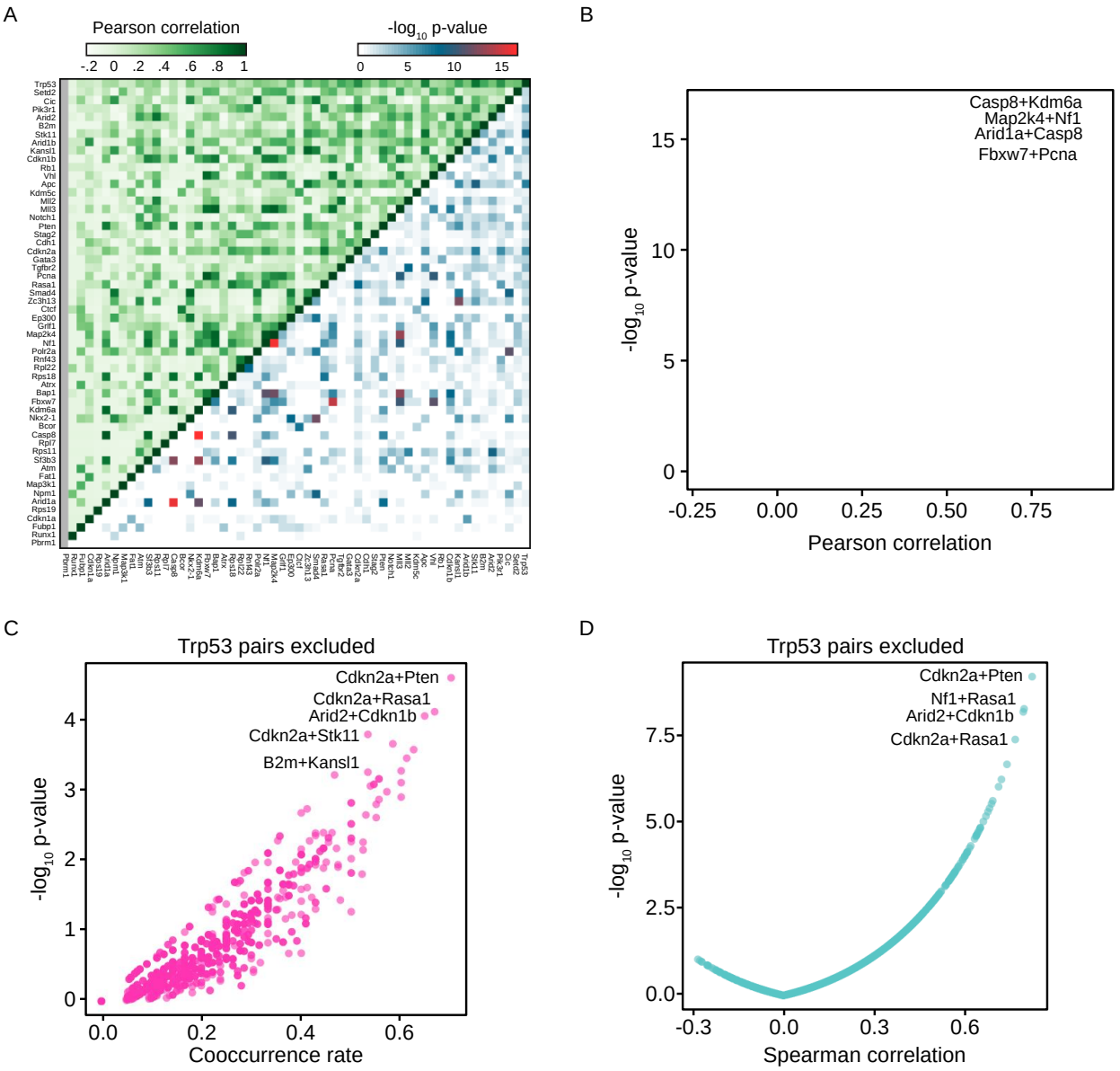
A
Pearson correlation
-.2 0 .2 .4 .6 .8 1
-log10 p-value
0 5 10 15
B
Casp8+Kdm6a
Map2k4+Nf1
Arid1a+Casp8
Fbxw7+Pcna
-log10 p-value
Pearson correlation
C
Trp53 pairs excluded
Cdkn2a+Pten
Cdkn2a+Rasa1
Arid2+Cdkn1b
Cdkn2a+Stk11
B2m+Kansl1
-log10 p-value
Cooccurrence rate
D
Trp53 pairs excluded
Cdkn2a+Pten
Nf1+Rasa1
Arid2+Cdkn1b
Cdkn2a+Rasa1
-log10 p-value
Spearman correlation

fig. S8. Additional co-mutation analysis. (**A**) Upper-left triangle: heat map of the pairwise Pearson correlation of sum % variant frequency for each gene, averaged across sgRNAs. Lower-right triangle: heat map of $-\log_{10}$ p-values by t-distribution to evaluate the statistical significance of the pairwise correlations. (**B**) Scatterplot of the Pearson correlation for each gene pair, plotted against $-\log_{10}$ p-values. (**C**) Scatterplot of the cooccurrence rates for each gene pair, excluding all pairs involving *Trp53*, plotted against $-\log_{10}$ p-values by hypergeometric test. (**D**) Scatterplot of the Spearman correlations for each gene pair, excluding all pairs involving *Trp53*, plotted against $-\log_{10}$ p-values.

Figure S9

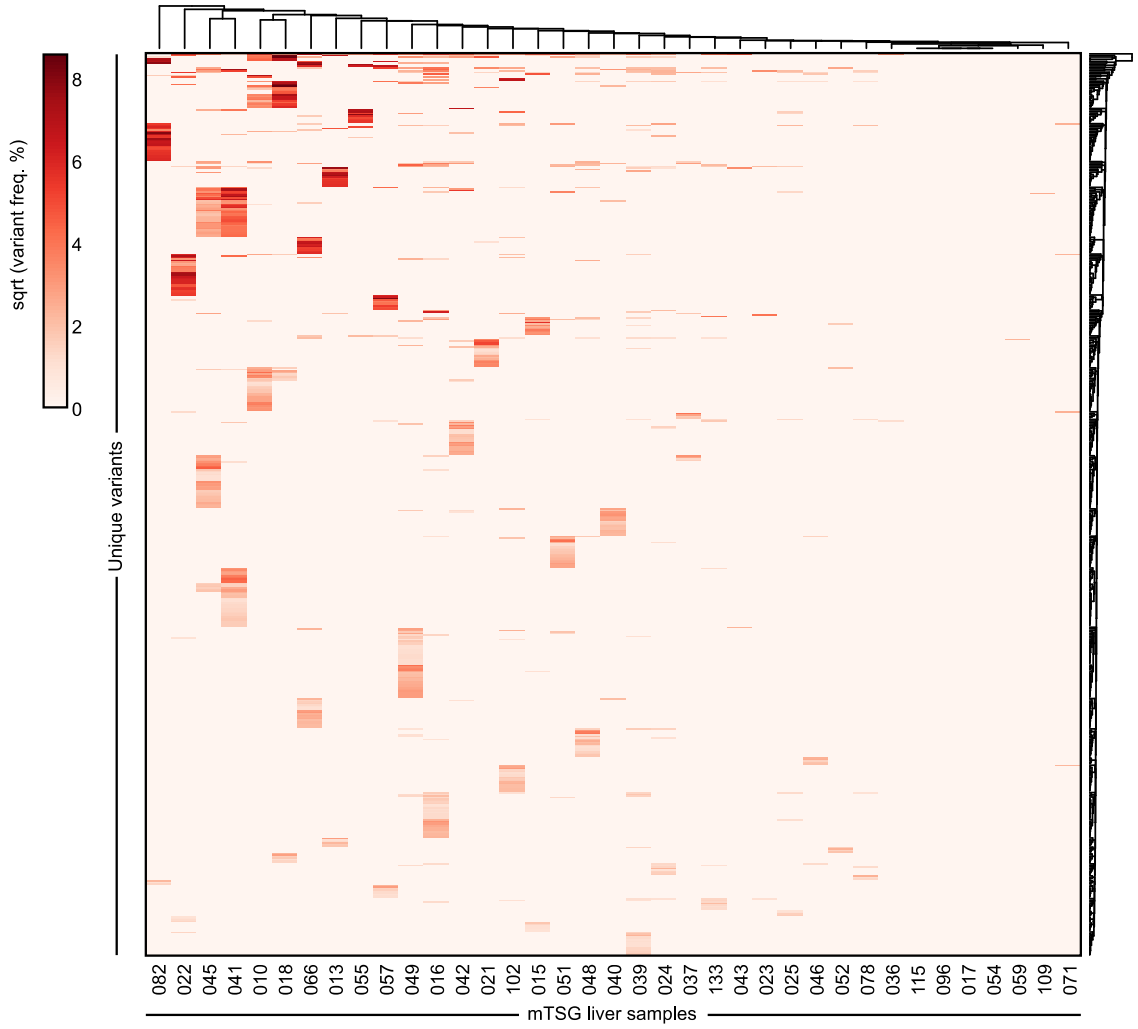
sqrt (variant freq. %)
8
6
4
2
0
Unique variants
082
022
045
041
010
018
066
013
055
057
049
016
042
021
102
015
051
048
040
039
024
037
133
043
023
025
046
052
078
036
115
096
017
054
059
109
071
mTSG liver samples

fig. S9. Heat map of all unique variants across all mTSG liver samples. Variant frequencies for all unique variants identified across mTSG liver samples, after square-root transformation for visual clarity. Rows denote unique variants, while columns denote different liver samples. Data was clustered using Euclidean distance and average linkage. 70.15% (416/593) of the variants were sample-specific, while 29.85% (177/593) variants were found across multiple samples.

Figure S10

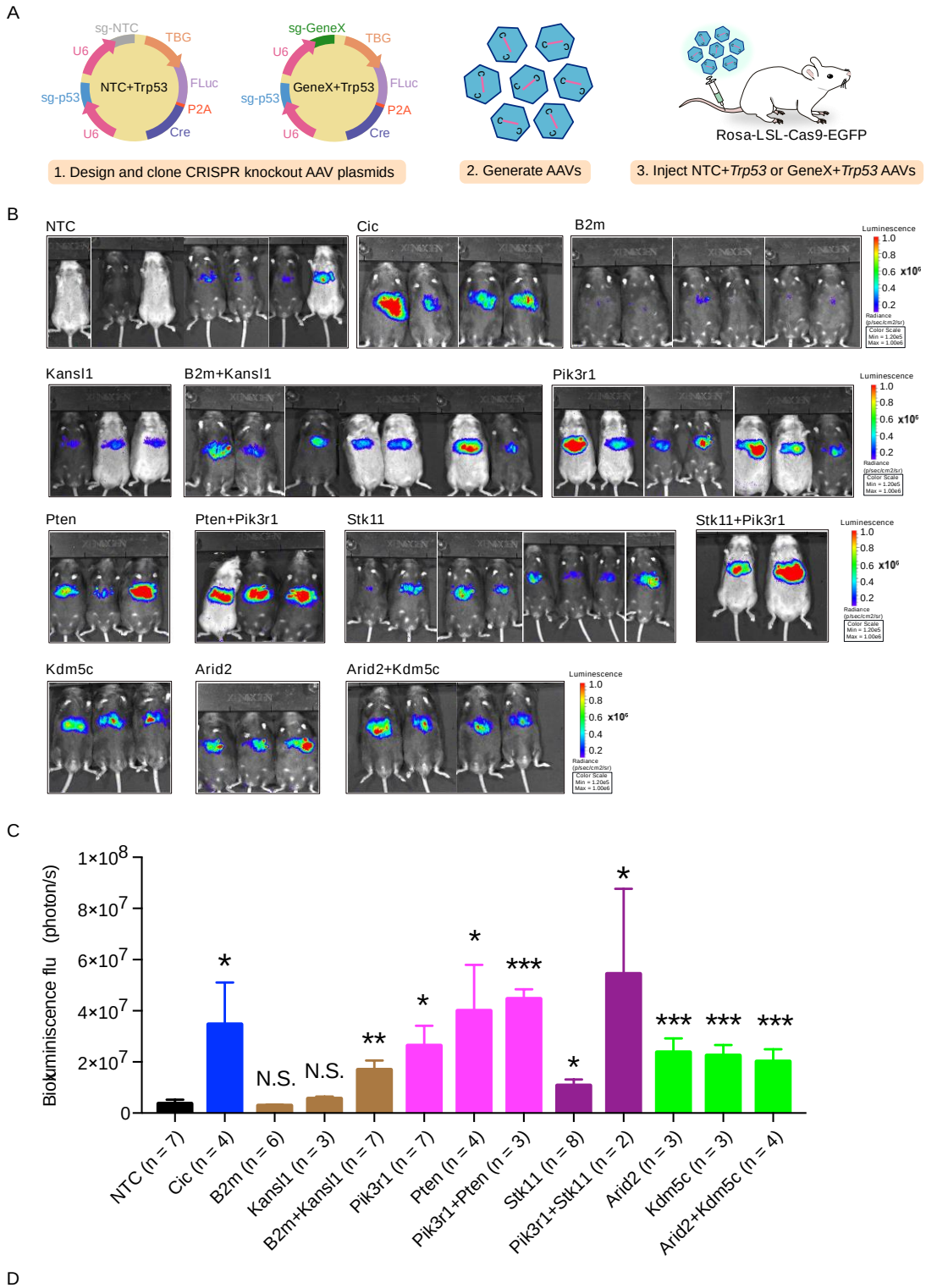
A
sg-NTC
TBG
U6
NTC+Trp53
FLuc
sg-p53
P2A
U6
Cre
sg-GeneX
TBG
U6
GeneX+Trp53
FLuc
sg-p53
P2A
U6
Cre
Rosa-LSL-Cas9-EGFP
1. Design and clone CRISPR knockout AAV plasmids
2. Generate AAVs
3. Inject NTC+Trp53 or GeneX+Trp53 AAVs
B
NTC
Cic
B2m
Kansl1
B2m+Kansl1
Pik3r1
Pten
Pten+Pik3r1
Stk11
Stk11+Pik3r1
Kdm5c
Arid2
Arid2+Kdm5c
Luminescence
C
Bioluminiscence flu (photon/s)
N.S.
N.S.
NTC (n = 7)
Cic (n = 4)
B2m (n = 6)
Kansl1 (n = 3)
B2m+Kansl1 (n = 7)
Pik3r1 (n = 7)
Pten (n = 4)
Pik3r1+Pten (n = 3)
Stk11 (n = 8)
Pik3r1+Stk11 (n = 2)
Arid2 (n = 3)
Kdm5c (n = 3)
Arid2+Kdm5c (n = 4)
D
Bioluminiscence flux (photon/s)
Days post-injection
NTC (n = 7)
B2m (n = 6)
Kansl1 (n = 3)
B2m+Kansl1 (n = 7)
Pik3r1 (n = 7)
Pten (n = 4)
Pik3r1+Pten (n = 3)
Stk11 (n = 8)
Stk11+Pik3r1 (n = 2)
Cic (n = 4)
Arid2 (n = 3)
Kdm5c (n = 4)
Kdm5c+Arid2 (n = 4)

fig. S10. Investigation and comparison of single or combinatorial knockout of screened TSGs in liver tumorigenesis. (**A**) Schematics of the design and cloning of liver-specific AAV-CRISPR vectors to functionally study target genes for their potential roles as independent and synergistic drivers of liver tumor in immunocompetent mice. The AAV-CRISPR plasmids contain two U6 promoter-driving sgRNA expression cassettes, with the 1st sgRNA targeting *Trp53,* and another one either as a non-targeting sgRNA (NTC + *Trp53*) or a geneX-targeting sgRNA (GeneX + *Trp53*). The plasmids also contained a liver-specific TBG promoter driving a co-cistronic expression cassette of firefly luciferase (FLuc) and Cre recombinase. AAVs were generated with these plasmids and injected intravenously into LSL-Cas9 mice**.** (**B**) Representative bioluminescence images of LSL-Cas9 mice injected with AAV9 that contains liver-specific TBG promoter-driving Cre and CRISPR dual-sgRNAs expression cassettes. Undetectable or weak luciferase activity was detected in NTC + *Trp53* AAV treated mice (n = 8) at 121 days post-injection, whereas persistent and robust luciferase activity was detected in the mice that were injected with the top scoring genes (GeneX + *Trp53*) or the highly co-mutated gene pairs from the screen. (**C**) Quantification of bioluminescence intensities of AAV-CRISPR injected LSL-Cas9 mice at 121 days post-injection are shown in units of photons/sec/cm^2/sr (Data represented as mean ± SEM). The mice that were injected with AAVs targeting the top screened genes or the highly correlated gene pairs had robust luciferase activity after 121 days of injection, indicating the role of these TSGs in accelerating development of tumors compared to NTC controls (two-sided unpaired *t* test, N.S. $p > 0.05$, * $p < 0.05$, ** $p < 0.01$, *** $p < 0.001$). In comparison to NTC (n = 7), *Cic* (n = 4, $p = 0.018$), *Pik3r1* (n = 7, $p = 0.015$), *Pten* (n = 4, $p = 0.011$), *Stk11* (n = 8, $p = 0.03$), *Arid2* (n = 3, $p = 0.001$) and *Kdm5c* (n = 3, $p = 0.0005$) knockout had significantly higher bioluminescence intensities. Double knockout of *Pik3r1+Pten* (n = 3) had significantly stronger luciferase activity compared to NTC (two-sided unpaired t test, $p < 0.0001$), but was not significantly different from knocking out *Pik3r1* or *Pten* alone (two-sided unpaired t test, N.S.). Double knockout of *Pik3r1+Stk11* (n = 2) had significantly stronger luciferase activity compared to NTC (two-sided unpaired *t* test, $p = 0.01$), but was not significantly different from knocking out *Pik3r1* or *Stk11* alone (two-sided unpaired *t* test, N.S.). In contrast, double knockout of *B2m+Kansl1* led to significantly higher luminescence intensities compared to NTC (two-sided unpaired *t* test, $p = 0.005$), *B2m* alone ($p = 0.001$) and *Kansl1* alone ($p = 0.02$). (**D**) Longitudinal IVIS live imaging of single or combinatorial AAV-CRISPR knockout of TSGs in driving liver tumorigenesis. The bioluminescence intensities of LSL-Cas9 mice injected with liver-specific AAVs containing either NTCs or sgRNAs targeting single gene or combinations of two genes. Left to right, *B2m + Kansl1, Pik3r1 + Pten, Pik3r1 + Stk11,* and *Arid2 + Kdm5c.*

Figure S11

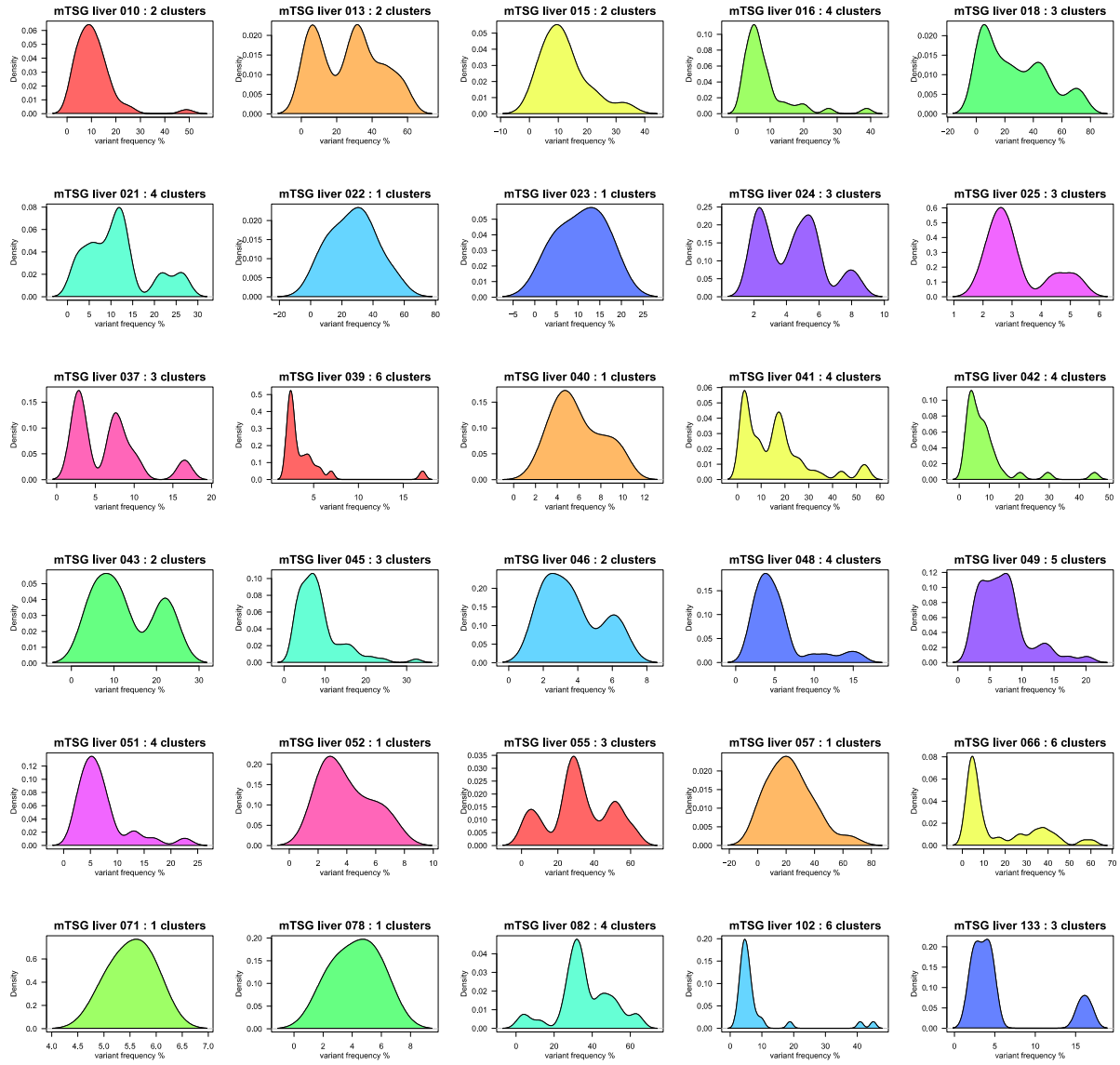
mTSG liver 010 : 2 clusters
mTSG liver 013 : 2 clusters
mTSG liver 015 : 2 clusters
mTSG liver 016 : 4 clusters
mTSG liver 018 : 3 clusters
mTSG liver 021 : 4 clusters
mTSG liver 022 : 1 clusters
mTSG liver 023 : 1 clusters
mTSG liver 024 : 3 clusters
mTSG liver 025 : 3 clusters
mTSG liver 037 : 3 clusters
mTSG liver 039 : 6 clusters
mTSG liver 040 : 1 clusters
mTSG liver 041 : 4 clusters
mTSG liver 042 : 4 clusters
mTSG liver 043 : 2 clusters
mTSG liver 045 : 3 clusters
mTSG liver 046 : 2 clusters
mTSG liver 048 : 4 clusters
mTSG liver 049 : 5 clusters
mTSG liver 051 : 4 clusters
mTSG liver 052 : 1 clusters
mTSG liver 055 : 3 clusters
mTSG liver 057 : 1 clusters
mTSG liver 066 : 6 clusters
mTSG liver 071 : 1 clusters
mTSG liver 078 : 1 clusters
mTSG liver 082 : 4 clusters
mTSG liver 102 : 6 clusters
mTSG liver 133 : 3 clusters
Density
variant frequency %

fig. S11. Mutant clonality and clustering analysis. Gaussian kernel density estimate of variant frequencies within each mTSG liver sample. The number of peaks in the kernel density estimate is an approximation for the clonality of each sample. From this analysis, most (24/30) samples appeared to be composed of multiple clones, with six monoclonal samples.

Supplementary tables: